Functional Conversion Between A-Type and Delayed Rectifier K$^+$ Channels by Membrane Lipids

Dominik Oliver, Cheng-Chang Lien, Malle Soom, Thomas Baukrowitz,
Peter Jonas, Bernd Fakler

Supporting Online Material

Methods

Molecular biology and biochemistry

Site-directed mutagenesis, in vitro mRNA synthesis, and oocyte injections were performed as described previously (*1*) in accordance with national and institutional animal research guidelines. The Kv channel subunits used were Kv1.1 (acc.no. X12589), Kvβ1.1 (X70662), Kv1.4 (M32867), Kv3.1 (NM_012856; gift of Dr. S. Grissmer), Kv3.2 (NM_139217), Kv3.4 (X62841), Kv4.3 (U75448; gift of Dr. M. Covarrubias), *Shaker* (NM_167595), BK (L16912; gift of Dr. L. Salkoff), and KCNQ2, KCNQ3 (Y15065, NM_004519; gift of Dr. T. Jentsch). The Kv3.4 ball domain was synthesized by conventional solid-phase synthesis, purified by HPLC, and dissolved into intracellular solution at a concentration of 10 μM (*2*).

Giant patch recording of recombinant Kv channels

Recordings from giant inside-out and outside-out patches excised from *Xenopus* oocytes were performed at room temperature (22 - 24 °C) as described previously (*3*). Currents were recorded with an EPC9 amplifier, low-pass filtered at 1-3 kHz, and sampled at 5-10 kHz. For inside-out patches, pipettes (0.2 - 0.4 MΩ) were filled with extracellular solution (mM): 120 XCl, 10 HEPES, and 1 CaCl$_2$ (pH 7.2 with XOH), where X is K$^+$, Na$^+$, or NH$_4^+$ as indicated; usually X was 5 K$^+$/115 Na$^+$ or 20 K$^+$/100 Na$^+$.

Intracellular solutions applied via a gravity-driven multi-barrel pipette were composed as follows (mM): 100 XCl, 10 X$_2$EGTA, and 10 HEPES (pH 7.2 with XOH, X$_2$CO$_3$, or XHCO$_3$), where X is K$^+$, Na$^+$, Rb$^+$, Cs$^+$, NH$_4^+$, Tl$^+$ and/or N-methyl-D-glucamine (NMDG$^+$) as indicated. In recordings with N-type-inactivating Kv channels dithiothreitol (0.2 or 0.4 mM) was added to prevent redox modulation (*4*). For experiments with Tl$^+$, Cl$^-$ was substituted by NO$_3^-$ (except for 2 mM Cl$^-$) in all extra- and intracellular solutions. Similarly, for recordings of BK channels, solutions contained methanesulfonate instead of Cl$^-$ (except 2 mM Cl$^-$); CaCl$_2$ was added to the intracellular solutions to yield 10 μM free [Ca^{2+}], as verified by a Ca^{2+}-sensitive

electrode. In experiments with external and internal TEA, NaCl, or KCl was substituted by the respective amount of TEACl at the concentrations indicated. For intracellular solutions containing Mg^{2+}, $MgCl_2$ was added to yield the free $[Mg^{2+}]$ indicated. For outside-out patch recordings the pipette and bath solutions were reversed.

Nucleated patch recording from interneurons and dynamic-clamp technique

Nucleated patch recordings from OA interneurons were performed at room temperature (21 - 24 °C) as described previously (*5, 6*). Transverse hippocampal slices of 300 µm thickness were cut from brains of 17- to 22-day-old Wistar rats. Recordings were made from visually identified interneurons with horizontal dendrites in *stratum oriens-alveus* in the CA1 subfield, using a Multiclamp 700A amplifier. Currents or voltages were low-pass filtered at 5 kHz and sampled at 10 kHz.

Extracellular solution used for slice superfusion contained (mM): 125 NaCl, 25 $NaHCO_3$, 2.5 KCl, 1.25 NaH_2PO_4, 2 $CaCl_2$, 1 $MgCl_2$, and 25 glucose, equilibrated with 95% O_2 / 5% CO_2. The extracellular solution used for nucleated patch recording contained (mM): 135 NaCl, 2.5 KCl, 2 $CaCl_2$, 1 $MgCl_2$, 30 glucose, and 5 HEPES (pH 7.2 with NaOH). Recording pipettes were filled with internal solution, containing (mM): 140 KCl, 10 K_2EGTA, 2 $MgCl_2$, 2 Na_2ATP, and 10 HEPES (pH 7.3 with KOH). Application of lipids was performed via bath superfusion.

To confer excitability to nucleated patches, artificial voltage-gated Na^+ conductances and leak conductances were added by dynamic clamp (*7*). Hard- and software was similar to that used previously (*6*). Briefly, a digital signal processor (DSP) board (equipped with 16-bit ADCs and DACs) was driven by a home-made program written in C. Calculations were performed in a timer- and interrupt-driven procedure, executed at a frequency of 60 kHz. Voltage-dependent Na^+ channels were represented by a Hodgkin-Huxley model of the form $I_{Na}(V) = G_{max} m^3 h (V - V_{Na})$, where G_{max} is the maximal conductance (set to values of 70 - 90 nS) and V_{Na} is 55 mV. In comparison to a previously reported model, the inactivation was right-shifted by 10 mV ((*8*); see (*9*)). Leak channels were implemented as $I_L = G_L (V - V_L)$, where G_L is the leak conductance (set to a value of 1 nS) and V_L is -70 mV. No voltage-gated K^+ channels were added to the nucleated patch.

Lipid handling

L-α-Phosphatidyl-D-myo-inositol-4,5-bisphosphate (PIP$_2$, Roche Molecular Diagnostics or Avanti Polar Lipids), L-α-Phosphatidylinositol-3,4,5-trisphosphate (PIP$_3$), L-α-Phosphatidylinositol-4-monophosphate (PIP) and L-α-

Phosphatidylinositol (PI) were dissolved in intracellular solution at a concentration of 1 mM, sonicated for 10 min in a cold water bath, aliquoted, and stored at -20°C. Samples were thawed on the day of use, sonicated for another 10 min, and diluted to their final concentration with intracellular solution.

AA and anandamide (Calbiochem or Sigma) were prepared as DMSO stocks (10 - 40 mM; final DMSO concentration ≤ 0.1 %) and stored at -20°C under nitrogen. Lipid-containing solutions were delivered to the application pipette via polyethylene or teflon tubings. The latter were found to provide a somewhat higher apparent concentration of fatty acids presumably due to their inert surface properties.

In-vitro liposome binding assay

Proteins and liposomes were prepared and assayed as described (10). Briefly, GST, GST-fused Kv1.4(1-75), and Kv3.4(1-40) proteins were overexpressed in *E.coli* strain BL-21 Codon Plus and immobilised on GSH-Sepharose according to manufacturer's instructions. Mixed liposomes were prepared from PIP_2, phosphatidylcholine (PC) and rhodamin-phosphatidylethanolamine (Rh-PE) to obtain lipid compositions of 0, 10, and 35 mol % PIP_2; the Rh-PE content was always 1 mol %. Immobilised proteins (0.01 mM) were incubated with liposomes and washed subsequently. Binding of liposomes to immobilised proteins was quantified by fluorescence measurements.

Data analysis

Inactivation was characterized either by the decay time constant (τ_{inact}) derived from a monoexponential fit to the decay phase of the current or by the ratio of currents remaining at time t after onset of the depolarizing pulse and the peak current (I_t/I_{max}). Steady-state current (I_{ss}, t = ∞) was determined from monoexponential fits. Inactivation of Kv1.4(K532V) in the presence of the Kv3.4 ball peptide and of Kv4.3 was better described by the sum of two exponential functions. For simplicity, only the predominant fast time constant (Kv1.4 K532V) or an approximative single time constant (Kv4.3) is reported.

Permeability ratios were determined from reversal potentials in biionic conditions (124 K_{ex} / 124 X_{in}) using equation (1)

$$V_{rev} = (RT/F) \ln((P_K[K]_o)/(P_X[X]_i)), \qquad (1)$$

where P_X/P_K is the ionic permeability ratio of cation X, and R, T, and F have their usual meanings.

Steady-state inactivation curves were obtained from the current response to a voltage step to 40 mV, following a conditioning pulse of 5 s to potentials between

-110 and -10 mV. Recovery from inactivation was examined with a protocol consisting of an inactivating pulse to 40 mV (100 ms), followed by an interval at -80 mV or -120 mV of exponentially increasing duration and a subsequent step to 40 mV to assess the fraction of channels that recovered from inactivation.

Curve fitting and further data analysis were done with Igor Pro 4.05A on a Macintosh G4 or PowerPC. Data are given as mean ± SD unless otherwise stated.

Supporting Figures

Fig. S1

Effect of PIP_2 on N-type inactivation occurs at physiological levels of the phosphoinositide.

A, Application of polyK to excised inside-out patches (25 µg/ml; 2-3 s) accelerated inactivation of Kv1.4(K532V) channels (left panel: representative experiment), indicating that phosphoinositides endogenously present in the oocyte membrane slowed N-type inactivation. Subsequent removal of polyK by heparin (100 µg/ml) restored the slower inactivation. Right panel summary of 8 experiments; data are mean ± SD.

B, Estimation of the amount of PIP_2 inserted into the patch membrane by application of exogenous PIP_2 using recombinant K_{ATP} channels as a PIP_2 sensor.

Inhibition of K_{ATP} channels by ATP is determined by the amount of phosphoinositides in the plasma membrane with increasing PIP_2 concentrations leading to a decreased ATP-inhibition (*11, 12*). In cardiac myocytes, the IC_{50} for ATP-inhibition of K_{ATP} channels was found to vary between 9 µM and 580 µM (102 excised patches; (*13*)), outlining the range of variation in naturally occurring phosphoinositide concentration.

These values were used for quantification of the PIP_2 concentration resulting from application to excised patches: First, the IC_{50} value for ATP-inhibition of cardiac K_{ATP} channels (Kir6.2 + SUR1) expressed in *Xenopus* oocytes was determined before and after application of 10 µM PIP_2 to giant patches for 5, 10, 20 and 30s (grey and black symbols indicate individual measurements and the mean of 17 patches). These data were then compared to the range of ATP-inhibition observed in cardiac myocytes (horizontal lines).

The comparison demonstrated that PIP_2 applications of up to 15 s may be equivalent to the levels observed in native tissue.

C, Removal of N-type inactivation occurs within seconds of application of PIP_2 (10 µM). The time course of the PIP_2 effect observed with Kv1.4, Kv1.4(K532V),

Kv1.1+Kvβ1.1, Kv3.4, and *Shaker* channels was fitted with a monoexponential and yielded the time constants indicated (mean ± SD of 7, 8, 12, 9 and 7 experiments, respectively).

Fig. S2

AA-induced inactivation is not use-dependent, and its impairment by NH_4^+ is independent of the current direction.

A, Development of inactivation was independent of channel activation as monitored by applying AA (4 µM; inside-out) either while repetitively opening channels by pulses to 40 mV (grey, mean of 7 experiments) or while keeping channels closed at -120 mV (representative experiment; n = 3). Inactivation was equally fast when probed 30 s after beginning of AA application. Inset depicts traces recorded before and after a 30-s application of AA to a patch held at -120 mV.

B, Switching intracellular K^+ from 124 mM to 5 mM (substituted with impermeant NMDG) with NH_4^+ as the only permeant ion on the extracellular side (124 mM) allowed changing between an outward K^+ current and an inward NH_4^+ current at 20 mV. While the K^+ outward current promoted AA-induced inactivation, inactivation was largely abolished by the NH_4^+ inward current (upper panel). With K^+ as the only permeant ion carrying inward and outward current AA was equally effective (lower panel). Insets depict the normalized inward (black trace) and outward current (grey trace) of either experiment.

C, Plot of AA-induced inactivation (at 20 ms after the voltage step) observed with NH_4^+ flowing through the channel in inward (124 mM NH_4^+ ex / 5 mM K^+ in) and outward (5 mM K^+ ex / 124 mM NH_4^+ in) direction. Note that prevention of lipid-induced inactivation by NH_4^+ was equally effective in either case. Data points are mean ± SD of 6 experiments.

Fig. S3

Lipid-induced inactivation of native Kv channels controls the AP phenotype.

A, Left panel, currents through native Kv channels (predominantly Kv3) recorded in a nucleated patch isolated from an OA interneuron in response to test pulses to 70 mV (holding potential -90 mV, 50 ms prepulse to -50 mV) in control conditions and in the presence of 0.1 and 0.3 µM anandamide. Right panel, currents recorded in a nucleated patch as on the left (upper traces, control and 1 µM anandamide superimposed) in response to APs applied as voltage-clamp commands (lower trace). In control conditions, the mean amplitude of the 5th AP-induced current was

$68 \pm 5\%$ of the 1st. In contrast, in the presence of 1 μM anandamide the K^+ currents displayed pronounced cumulative inactivation with the same stimulus paradigm; the amplitude of the 5th AP-induced current was $26 \pm 4\%$ of the 1st (n = 3).

B, **C**, Anandamide-induced changes in the AP phenotype recorded in a nucleated patch as in A containing both endogenous Kv channels and artificial Na^+ channels generated by the dynamic-clamp technique (see Methods). Trains of APs were evoked by 150 ms depolarizing current pulses of 30 pA (B) and 70 pA (C) in the absence or presence of anandamide (0.1 or 0.3 μM). Upper traces are membrane potential recordings, lower traces are corresponding dynamic-clamp Na^+ currents (scale bar is 10 nA).

Fig. S4

Proposed molecular mechanisms of the lipid effects on Kv channel gating.

Phosphoinositides immobilize the positively charged ball domain and prevent it from entering the channel pore. Lipids such as AA (shown as stick model) and anandamide after inserting into the membrane from either side interact with the channel protein and thus allosterically induce rapid closure of the open Kv channel pore through conformational alterations in the selectivity filter. Inner pore and selectivity filter were taken from the structure of the open MthK-pore (*14*) with an AA molecule positioned equivalently to the fatty acid found in the KcsA structure (*15*). The ball structure was taken from Kv3.4 ((*16*) surface presentation and color coding as in Fig. 3); positioning of the Kv3.4 ball domain in the MthK-pore was obtained by molecular docking (*17*).
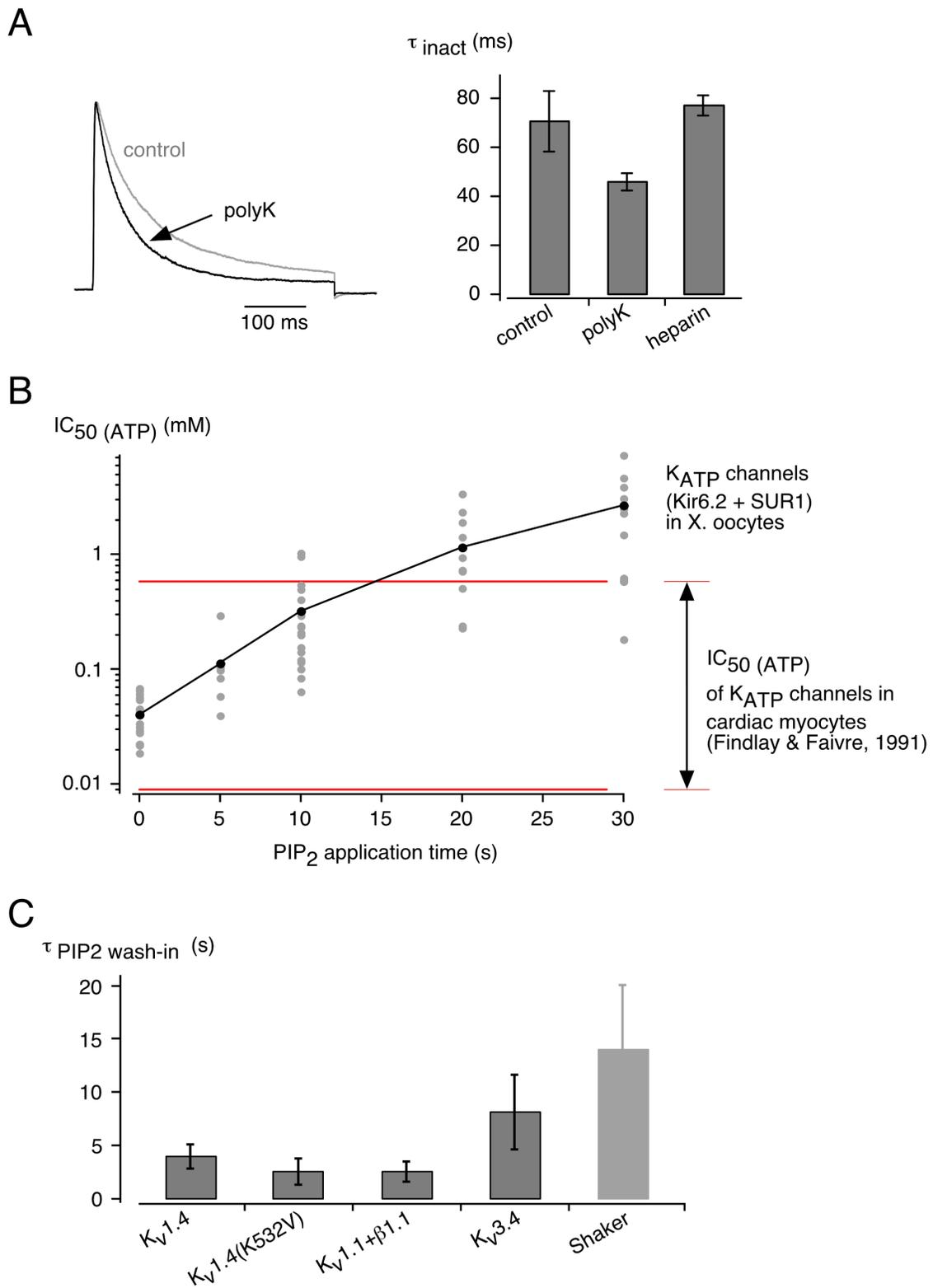
Figure S1, Oliver et al.

Figure S2, Oliver et al.

A

OA interneuron
(nucleated patch)

0.1 μM

0.3 μM

0.2 nA

20 ms

I (nA)

0.3

0.2

0.1

0

control

+ anandamide

V (mV)

20

-20

-60

25 ms

B

V (mV)

20

-20

-60

control

I (Na)

50 ms

V (mV)

20

-20

-60

0.1 μM anandamide

V (mV)

20

-20

-60

0.3 μM anandamide

30 pA

C

70 pA
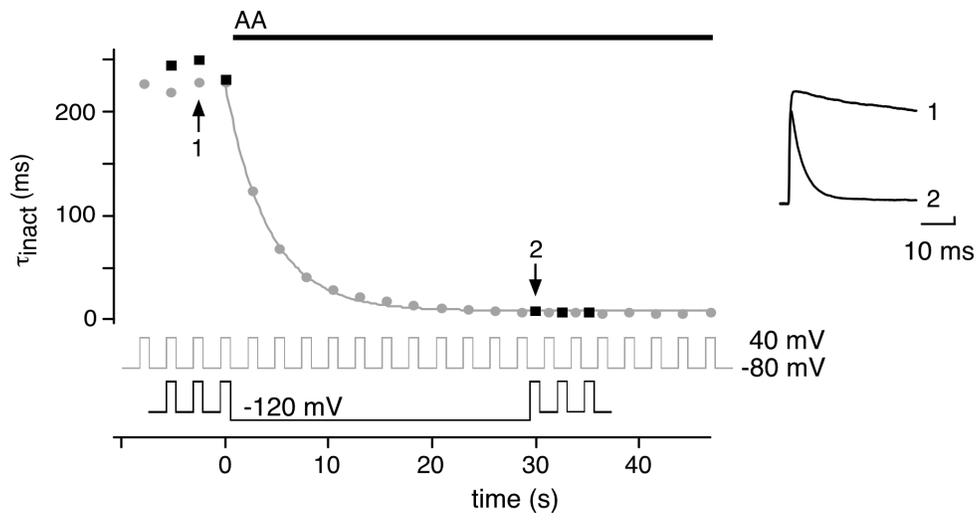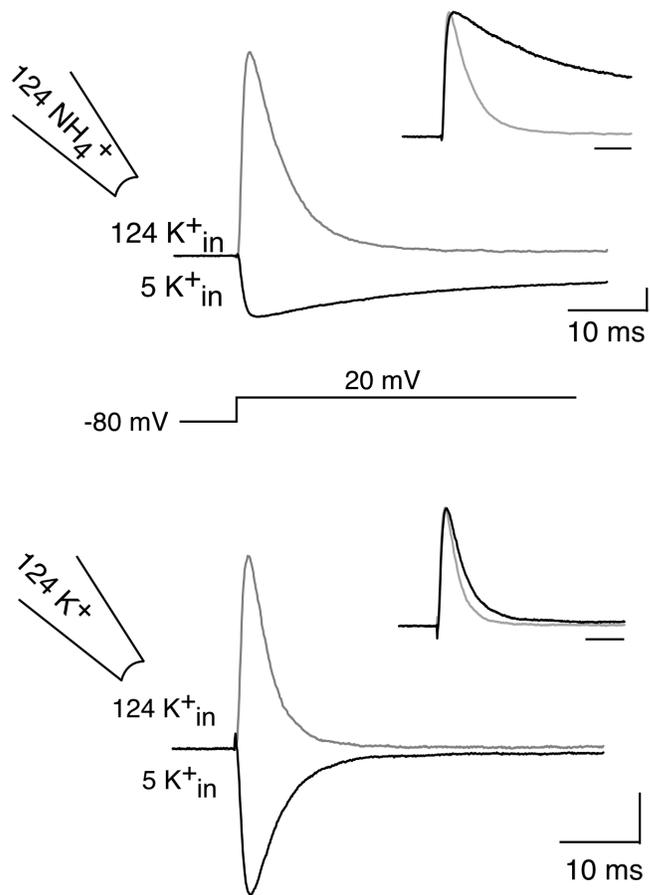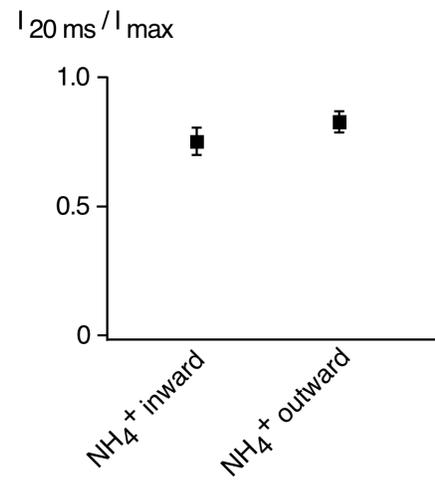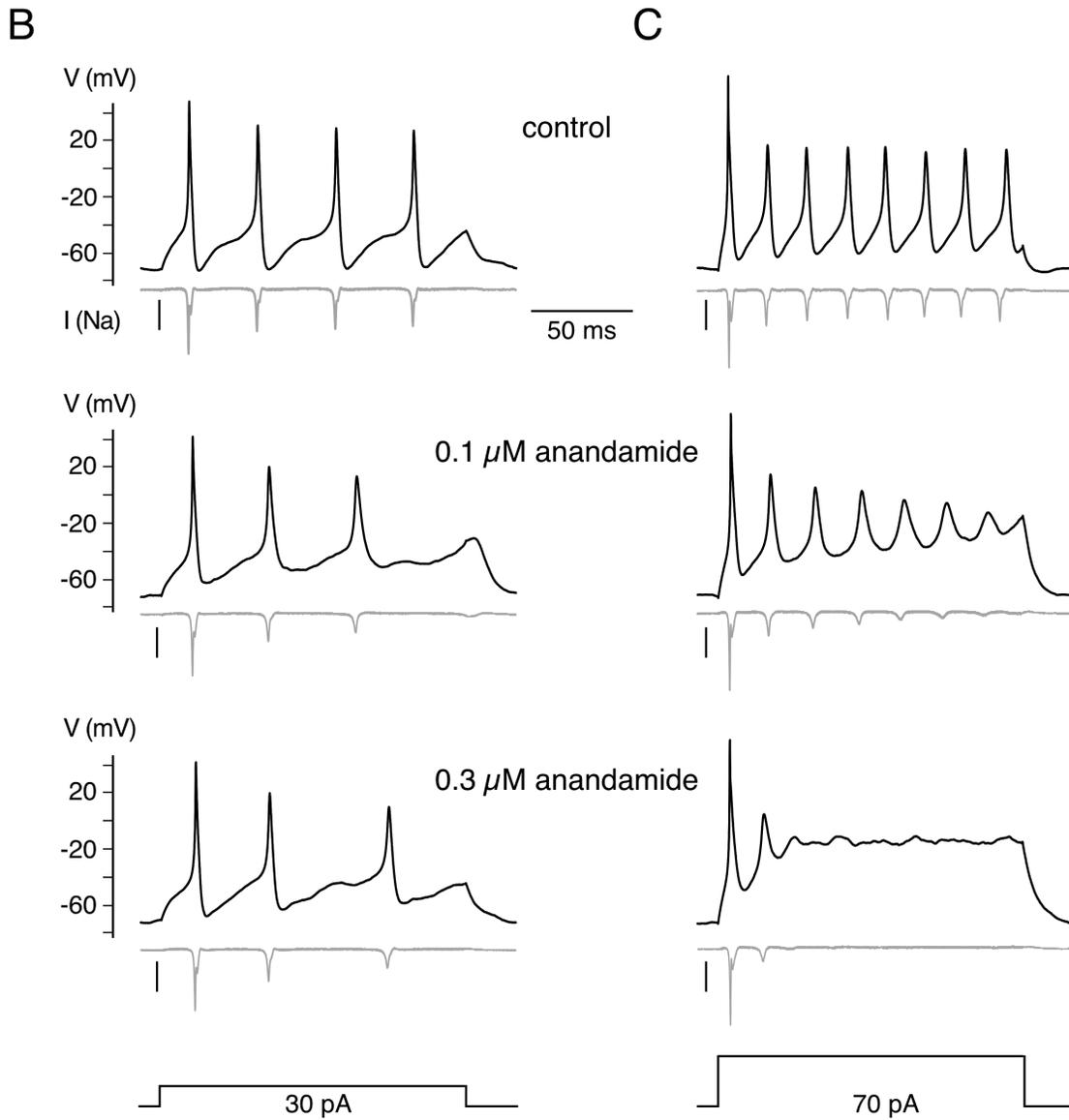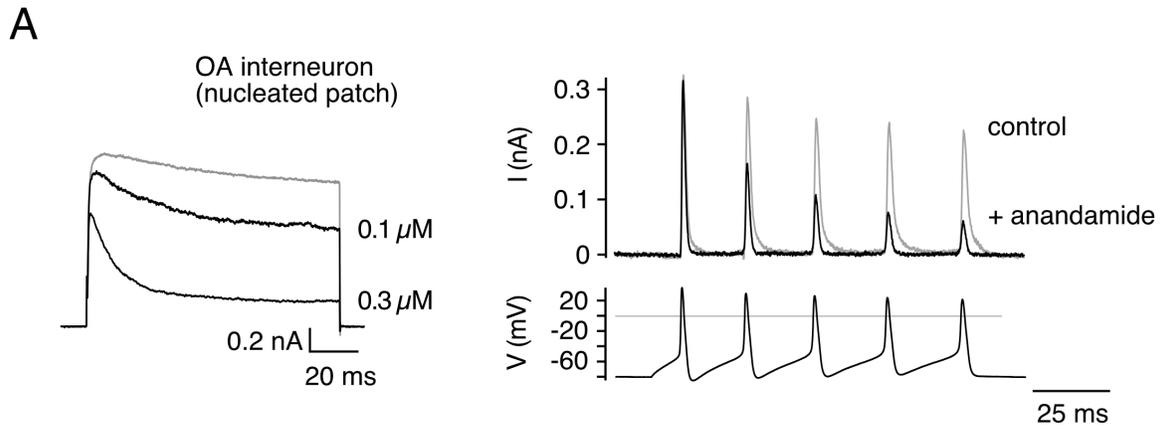
Figure S3, Oliver et al.
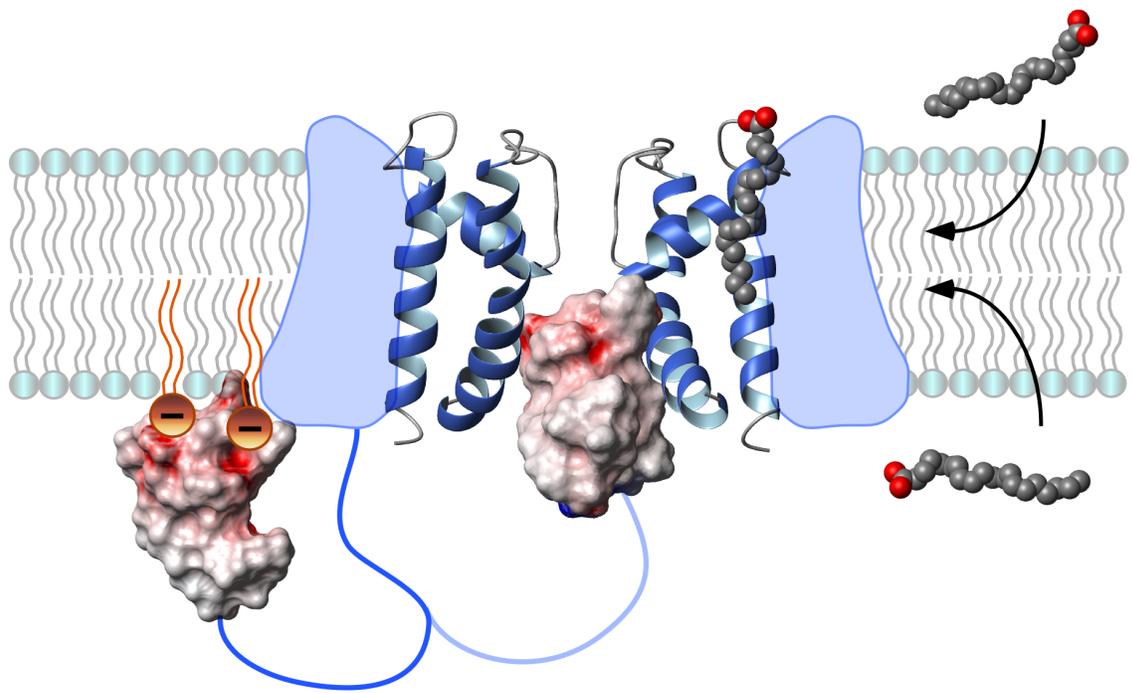
Figure S4, Oliver et al.

Supporting references and notes

1. B. Fakler, U. Brändle, E. Glowatzki, H. P. Zenner, J. P. Ruppersberg, *Neuron* **13**, 1413 (1994).
2. C. Antz *et al.*, *Nat. Struct. Biol.* **6**, 146 (1999).
3. B. Fakler *et al.*, *Cell* **80**, 149 (1995).
4. J. P. Ruppersberg *et al.*, *Nature* **352**, 711 (1991).
5. C. C. Lien, M. Martina, J. H. Schultz, H. Ehmke, P. Jonas, *J. Physiol.* **538**, 405 (2002).
6. C. C. Lien, P. Jonas, *J. Neurosci.* **23**, 2058 (2003).
7. A. A. Sharp, M. B. O'Neil, L. F. Abbott, E. Marder, *J. Neurophysiol.* **69**, 992 (1993).
8. A. Erisir, D. Lau, B. Rudy, C. S. Leonard, *J. Neurophysiol.* **82**, 2476 (1999).
9. M. Martina, I. Vida, P. Jonas, *Science* **287**, 295 (2000).
10. M. Soom *et al.*, *FEBS Lett.* **490**, 49 (2001).
11. T. Baukrowitz *et al.*, *Science* **282**, 1141 (1998).
12. S. L. Shyng, C. G. Nichols, *Science* **282**, 1138 (1998).
13. I. Findlay, J. F. Faivre, *FEBS Lett.* **279**, 95 (1991).
14. Y. Jiang *et al.*, *Nature* **417**, 523 (2002).
15. D. A. Doyle *et al.*, *Science* **280**, 69 (1998).
16. C. Antz *et al.*, *Nature* **385**, 272 (1997).
17. R. Wissmann *et al.*, *J. Biol. Chem.* **278**, 16142 (2003).